Optical properties and electronic structure of MgAuSn

S. J. Lee
Ames Laboratory, Iowa State University, Ames, Iowa 50011

J. M. Park, T. A. Wiener, L. L. Miller, and D. W. Lynch
Ames Laboratory and Department of Physics and Astronomy, Iowa State University, Ames, Iowa 50011
(Received 18 June 2001; published 10 September 2001)

The optical conductivity spectrum of single-crystal MgAuSn was measured by spectroscopic ellipsometry in the energy range 1.5–5.0 eV. The spectrum has a large peak at 2.9 eV and a small shoulder around 4.3 eV. The band structure, density of states, and interband contribution to the optical conductivity were calculated with the tight-binding linear muffin-tin orbital method in the atomic-sphere approximation. The intraband contribution to the optical conductivity was added using the Drude response fitted to the experimental data. The total theoretical spectrum, including the intraband contribution, agrees well with experimental data.

DOI: 10.1103/PhysRevB.64.125112 PACS number(s): 78.20.−e, 71.20.Lp, 71.15.Ap

I. INTRODUCTION

Optical properties, such as reflectivity, color, dielectric function, and skin depth, provide useful information in characterizing materials. The optical response to incident light, especially in the visible range, involves interband transitions of bound electrons from occupied states below the Fermi energy to empty states above. The intraband contribution to the optical response, which is important in the infrared region, can be treated classically within the framework of the Drude model, based on the motion of free electrons. The optical properties of MgAuSn are interesting because it shows a purple color. These optical properties can be explained by a combination of a first-principles calculations and the phenomenological Drude model. As far as we know, there has been no theoretical calculation on MgAuSn, which is essential for the interpretation of the optical spectrum. In this paper we present ellipsometric measurements of the optical conductivity of MgAuSn and calculations of the real part of the diagonal conductivity, the density of states (DOS) and the band structures of MgAuSn obtained by the tight-binding linear muffin-tin orbital (TB-LMTO) method. For the fit of the dispersive part of the optical spectrum in the lower-energy region, the Drude model is employed. The sum of the two calculated contributions agrees well with the experimental data. Drews *et al.*[1] measured the reflectivity of ternary and quaternary colored compounds of MgAB (A = Pd, Pt, B = Sb, Sn) and LiMgCSn (C = Pd, Pt) with the same structure as our samples. They used mechanically polished polycrystalline samples in the energy range of 0.5–4.0 eV. No peak was observed in the reflectivity spectra between 3.0 and 4.0 eV while our measurement for MgAuSn shows a noticeable peak at 3.5 eV. The first-principles calculation also predicts a large peak in this energy region. Mechanical polishing may have caused the loss of a possible peak. Our sample was a single crystal with a good surface quality; no mechanical polishing or etching was performed before the optical measurement.

II. EXPERIMENT

A. Sample preparation and characterization

Large single crystals of MgAuSn were grown by a self-flux technique.[2] Starting elements, magnesium (99.98% purity), gold (99.99% purity), and tin (99.8% purity) were sealed into a tantalum crucible in the ratio of $Mg_{0.36}Au_{0.10}Sn_{0.54}$. This was done in order to minimize the loss of magnesium due to its high vapor pressure. The crucible was then sealed into a quartz ampoule with a partial pressure of argon. This ampoule was placed in a box furnace and heated to 800 °C. The melt was cooled to 650 °C over a period of 2 h then cooled to 500 °C over a period of 60 h. At this temperature the crystals were separated from the remaining melt by inverting the ampoule and spinning in a centrifuge, forcing the still-liquid flux out through quartz wool which was filled above the crucible. The quartz wool in the crucible acts as the filter during the flux removal.

Crystals grown in this way display an octahedral morphology and a typical size of 125 mm^3. MgAuSn crystallizes in the cubic AlLiSi ($F\bar{4}3m$) structure as shown in Fig. 1. The sites (000), ($\frac{1}{4}\frac{1}{4}\frac{1}{4}$), and ($\frac{1}{2}\frac{1}{2}\frac{1}{2}$) are occupied by Sn, Au, and Mg, respectively. The Au and Sn sublattices form the zinc-blende structure. The surface of the as-grown samples was clean and flat enough to use for optical measurements without further mechanical or chemical treatment. Cu-$K\alpha$ x-ray data on crushed MgAuSn single crystals were collected at room temperature. Rietveld refinement[3] of the crystallographic parameters was made using Si as an internal standard. A 3% impurity level is estimated from peak heights of the nonindexed peaks. The lattice constant was determined as 6.419 Å, which agrees with the previously reported result[4] of 6.41 Å.

For electrical resistivity measurements, single crystals were cut to form a bar using a wire saw. Typical bar lengths were 2–3 and 0.5 mm in width and thickness. The electrical resistivity ρ was measured between 1.8 and 300 K using a standard four-probe technique, with an LR400 ac bridge operating at 16 Hz and an excitation current of 3 mA. Electrical

 ©2001 The American Physical Society

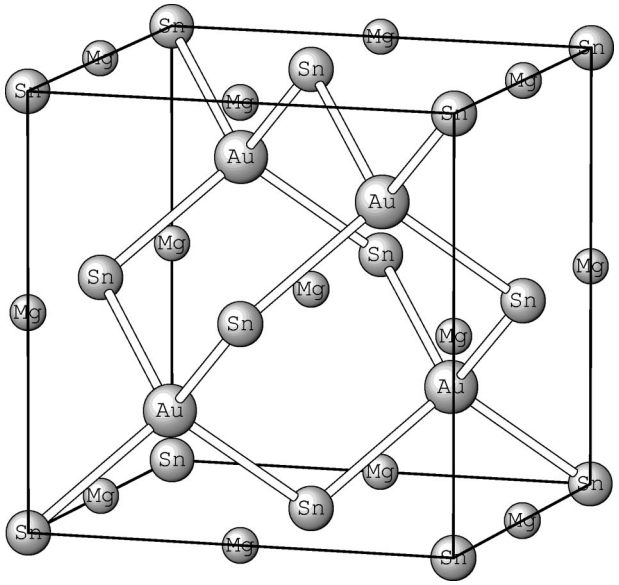

FIG. 1. Crystal structure of MgAuSn.

contact was made to the samples using epoxy, with typical contact resistances of 1–2 Ω. Due to the uncertainty of the bar dimensions and the contact separation, there is an approximate uncertainty of ±10% in the absolute values of the resistivity obtained for the sample. The resistivity versus temperature plot of MgAuSn shows typical metallic behavior. The resistivities at 2 and 300 K are 3.1 and 11.1 μΩ cm, respectively. The residual resistivity ratio, $\rho(300\ \mathrm{K})/\rho(4.2\ \mathrm{K})$, is 3.58, which indicates that the quality of the sample is acceptable. dc magnetization was measured using a commercial Quantum Design superconducting quantum interface device (SQUID) magnetometer, in a variety of applied fields up to 5.5 T and temperatures from 1.8 to 350 K. The magnetization measurements show a typical diamagnetic character.

B. Ellipsometry

Ellipsometry is widely used to characterize surfaces, interfaces, and thin films. Ellipsometry[5] is based on the fact that the state of polarization of light is changed on reflection. This change is directly related to the dielectric function of the reflecting material. With rotating analyzer ellipsometry (RAE),[6] one measures the complex ratio of the reflection coefficients defined by

$$\tilde{\rho}=\frac{r_p}{r_s}=\left|\frac{r_p}{r_s}\right|e^{i\Delta}=\tan\Psi e^{i\Delta}, \tag{1}$$

where r_p, r_s are the complex amplitude reflection coefficients for *p*- and *s*-polarized light, and Ψ and Δ express the change in amplitude and phase between *p* and *s* components of polarized light reflected from a surface. Ψ and Δ are quantities directly measurable from ellipsometry. For a bulk sample without surface overlayers, the complex dielectric function $\tilde{\varepsilon}$ is related to the complex reflectivity ratio $\tilde{\rho}$ by

$$\tilde{\varepsilon}=\sin^2\phi_0+\sin^2\phi_0\tan^2\phi_0\left[\frac{1-\tilde{\rho}}{1+\tilde{\rho}}\right]^2, \tag{2}$$

where ϕ_0 is the angle of incidence, 68° in this experiment. From this dielectric function $\tilde{\varepsilon}=\varepsilon_1+i\varepsilon_2$, the complex optical conductivity $\tilde{\sigma}=\sigma_1+i\sigma_2$ can be obtained by

$$\tilde{\varepsilon}=1-\frac{4\pi\tilde{\sigma}i}{\omega}. \tag{3}$$

The absorptive component of the optical conductivity σ_1 is related to the imaginary part of the dielectric function ε_2 by $\sigma_1=\omega\varepsilon_2/4\pi$.

Equation (2) is obtained using the two-phase model assuming that the system consists of an isotropic ambient and an isotropic semi-infinite, homogeneous solid. But in real situations, there is a surface overlayer of certain thickness on the top of the single crystal. We have studied the overlayer problem on single crystals of $LuAl_2$ and $YbAl_2$ by using a three-phase model, air-overlayer-bulk single crystal.[7] In order to estimate the optical conductivity (dielectric function) of clean bulk $LuAl_2$ and $YbAl_2$ with the three-phase model, we assumed a constant effective refractive index for the complicated oxide layer. Correcting the data with a three-phase model, we found the oxide overlayer reduced the magnitude of the optical conductivity. We applied the same procedure to MgAuSn and the results are in the discussion section.

III. BAND-STRUCTURE CALCULATIONS

For our band-structure calculation, the tight-binding linear muffin-tin orbital (TB-LMTO) method based on the atomic-sphere approximation (ASA) with the inclusion of spin-orbit coupling is employed. The spin-orbit interaction lifts some of the degeneracies of the energy bands at high symmetry points or lines in *k* space. It couples the spin-up and spin-down states and doubles the size of the Hamiltonian matrix from that of the scalar-relativistic Hamiltonian matrix. For the TB-LMTO calculation, we used the room-temperature lattice constant of 6.419 Å for MgAuSn from the x-ray powder-diffraction pattern. In the vacant fcc sublattice site, an empty muffin-tin sphere with zero nuclear charge was inserted. The exchange-correlation potential is included in the local-density approximation (LDA) with the von Barth-Hedin form.[8] The *k*-integrated functions have been evaluated by the tetrahedron technique with 144 *k* points in the $\frac{1}{48}$ irreducible wedge of the Brillouin zone. Once the self-consistent potential and charge are obtained, the real part of the optical conductivity can be calculated. In cubic systems it is necessary to calculate only one of the three diagonal components of the conductivity tensor. We used Kubo's linear response theory,[9] which leads to interband contributions to the conductivity of the following form:

$$\sigma_{xx}=\frac{\pi e^2}{3m^2\omega}\sum_{f,i}\int_{BZ}d^3k\frac{2}{(2\pi)^2}|p_{fi}|^2\times f_i(k)\times[1-f_f(k)]$$
$$\times\delta[E_f(k)-E_i(k)-\hbar\omega], \quad (4)$$

where BZ denotes Brillouin zone, $f(k)$ is the Fermi distribution function and i, f stand for the occupied initial and unoccupied final energy band states at wave vector k, respectively.

$$p_{fi}=\frac{\hbar}{i}\langle f|\nabla|i\rangle \quad (5)$$

is the dipole matrix element between the occupied $E_i(k)$ and unoccupied $E_f(k)$ one-electron states. The so-called combined corrections were used for the matrix elements to improve the ASA by taking into account the real form of a cell. The calculated spectra are unbroadened quantities. To improve this formalism the interaction between correlated electrons as described by the quasiparticle picture was considered. This picture describes changes in the single-particle picture using self-energy terms. The self-energy is usually momentum and energy dependent and consists of two parts,[10]

$$\Sigma=\Sigma_1+i\ \Sigma_2. \quad (6)$$

The real part represents a shift of the one-electron energy of a state, while the imaginary part describes the broadening of the energy level caused by the finite lifetime of a state. To consider the broadened experimental optical conductivity, the theoretical optical conductivity was convoluted with an energy-dependent Lorentzian broadening function[11] of width equal to the imaginary part of the complex self-energy which was set to constant value of $\Sigma_2=0.2$ eV. The real part of the self-energy was not considered in this calculation because the shift of the theoretical peak positions from those of the experimental spectra is small (<0.3 eV). From the energy bands and the TB-LMTO eigenvectors, we calculated the total and orbital projected density of states. The complex dielectric function consists of two parts, intraband contributions from free carriers and interband contributions due to band-to-band optical transitions. The intraband term of the dielectric function can be described quantitatively within the framework of the Drude model[12] as

$$\varepsilon_1(\text{intraband})=1-\frac{\omega_p^2\tau^2}{1+\omega^2\tau^2},$$

$$\varepsilon_2(\text{intraband})=\frac{\omega_p^2\tau}{\omega(1+\omega^2\tau^2)}, \quad (7)$$

where $\omega_p=(4\pi Ne^2/m^*)^{1/2}$ is the plasma frequency and τ is a relaxation time for conduction-band electrons. N is the number density of free electrons and m^* is an effective mass of the electrons.

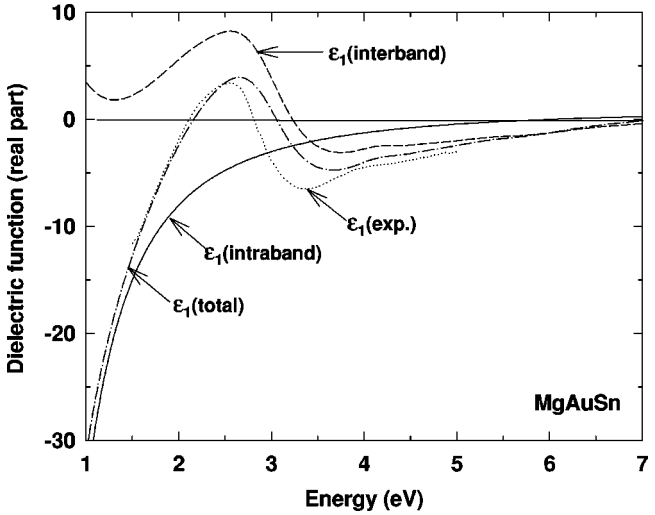

FIG. 2. Real part of the pseudodielectric function. Dotted: experiment; dashed: calculated interband contribution; solid: intraband contribution from the Drude model; dot-dashed: sum of the calculated interband contribution and the intraband contribution from the Drude model.

IV. RESULTS AND DISCUSSION

The experimental real and imaginary parts of the complex dielectric function are shown in Figs. 2 and 3 as dotted lines. The imaginary part of the dielectric function ε_2 from the TB-LMTO method in the local-density approximation, which contains only interband contributions, agrees well with the experimental data in the measured energy range. This is because the intraband contribution to ε_2 is very small in the visible and UV regions. The agreement between the experimental data and the calculated interband contributions of the real part of the dielectric function ε_1 is poorer, as shown in Fig. 2. The large negative intraband contribution to

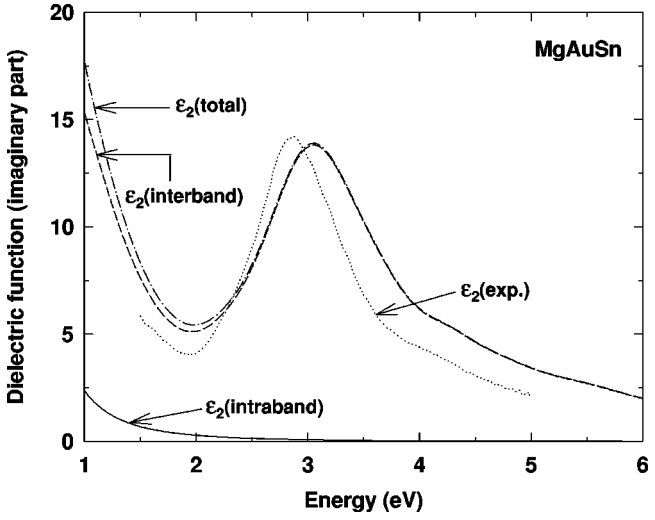

FIG. 3. Imaginary part of the pseudodielectric function. Dotted: experiment; dashed: calculated interband contribution; solid: intraband contribution from the Drude model; dot-dashed: sum of the calculated interband contribution and the intraband contribution from the Drude model.

ε_1 from the free electrons cannot be ignored for the photon energies below about 3.0 eV. The Drude model given in Eq. (7) contains two parameters, ω_p and τ. Typical plasmon energies $\hbar\omega_p$ and relaxation times for metals are of the order of a few eV and 10^{-14} s, respectively.[13] To carry out the estimation of the free electron contribution to ε_1, we varied the plasmon energy and scattering time until the total ε_1 (dot-dashed line in Fig. 2) fit the experimental data (dotted line in Fig. 2). The best-fit values for $\hbar\omega_p$ and τ were 6.0 eV and 1.0×10^{-14} s, respectively. The intraband contributions from these parameters are shown by solid lines in Figs. 2 and 3. The dot-dashed lines in Figs. 2 and 3 represent the total dielectric function from the interband and intraband parts, the dotted is for experimental data, the dashed is the calculated interband contribution. and the solid line is for the intraband contribution from the Drude model. The interband contribution to ε_1 at 2.5 eV is large enough to overcome the intraband contribution as shown in Fig. 2. As a result, the total ε_1 is positive between 2.2 and 3.0 eV. The sign of the experimental ε_1 is positive between 2.1 to 2.8 eV.

The dielectric function of MgAuSn resembles those of Cu, Au, and $AuAl_2$ (Refs. 14–19) because, with one exception, the electronic structures are similar. The bands within 2 eV of the Fermi level are nearly free-electron like, giving a prominent Drude term for energies below about 2 eV, with little (MgAuSn) or no (Cu, Au) interband contributions to ε_2, and a constant contribution to ε_1. Then at higher energies strong interband transitions begin. These are, at least in part, from the top of the 3*d* band (Cu) or 5*d* band (Au), but in MgAuSn the Au 5*d* states lie further below E_F than in Au and $AuAl_2$, and only inter-*s*-*p* band transitions occur below 5 eV. The interband transitions also affect the loss function, $\mathrm{Im}(-1/\tilde{\varepsilon})=\varepsilon_2/(\varepsilon_1^2+\varepsilon_2^2)$, in similar ways. Mazin *et al.* discussed in detail on the characteristic energy loss spectra in 4*d* metals from Y to Pd using the interband transition pictures within the density-functional technique.[20] The positive interband contributions to ε_1 cause the ε_1 spectrum to cross, or nearly cross, zero. If ε_2 is sufficiently small near this crossing, a well-defined peak in the loss function occurs. Such a ''screened plasmon'' peak is very prominent in the loss function spectrum of Ag, but in Cu and Au, ε_1 does not quite reach zero, and no well-defined peak occurs. A similar effect occurs in MgAuSn. A well defined peak occurs at 2.0 eV, near which ε_1 crosses zero and ε_2 is not too large.

The optical conductivity is related to the dielectric function by Eq. (3). The absorptive part of the optical conductivity is shown in Fig. 4. There are two peaks in the measured spectrum, a large one at 2.9 eV and a small one at 4.2 eV. The calculated σ_1 of the clean bulk MgAuSn obtained using the three-phase model for an assumed overlayer thickness of 10 Å with an effective refractive index 1.5 is shown as dot-dot-dashed line in Fig. 4. The magnitude of the optical conductivity of the clean bulk sample becomes enhanced 7.5% at the peak (2.9 eV) in the optical conductivity spectrum. To analyze the origin of these peaks, the electronic band structure and density of states were calculated using the TB-LMTO method. The electronic structure of MgAuSn is shown in Fig. 5 along the high-symmetry points in the Brillouin zone for the fcc lattice. The transitions around 2.9 eV occur near the lines *K*-*L* and *K*-Γ, while the transitions around 4.2 eV occur near the lines *X*-Γ and *X*-*W*. These transitions are marked as solid and dashed arrows in the electronic structure in Fig. 5, respectively. The occupied and unoccupied bands involved in the transition are primarily of Sn-*p*, Mg-*p*, and Au-*p* characters hybridized with Sn-*d*, Mg-*d*, and Au-*d* bands. The lowest occupied bands between -8 and -10 eV are primarily Au-*d* character hybridized with Mg-*p* states. The occupied bands between -4.5 and -6.5 eV are primarily of Au-*d* states hybridized with Sn-*p*

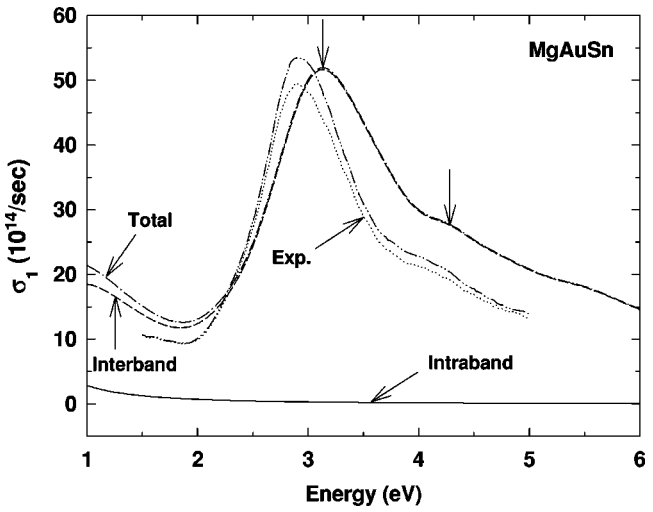

FIG. 4. Absorptive part of the optical conductivity σ_1. Dotted: experiment; dashed: calculated interband contribution; solid: intraband contribution from the Drude model; dot-dashed: sum of the calculated interband contribution and the intraband contribution from the Drude model; dot-dot-dashed: the calculated σ_1 of the clean bulk MgAuSn obtained using the three-phase model with a constant refractive index $n=1.5$ and thickness of 10 Å. Arrows in the dash-dotted curve show peaks in the optical conductivity.

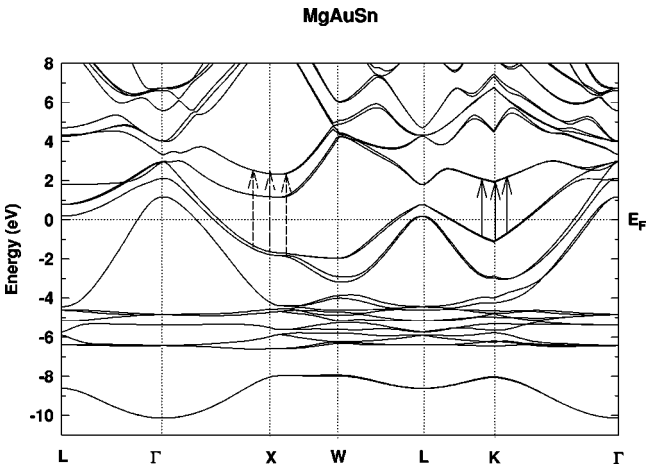

FIG. 5. Band structure along the high-symmetry lines for MgAuSn calculated from the TB-LMTO method with the LDA in the atomic-sphere approximation, including spin-orbit interaction. Strong direct interband transitions corresponding to the measured peaks are marked by arrows.

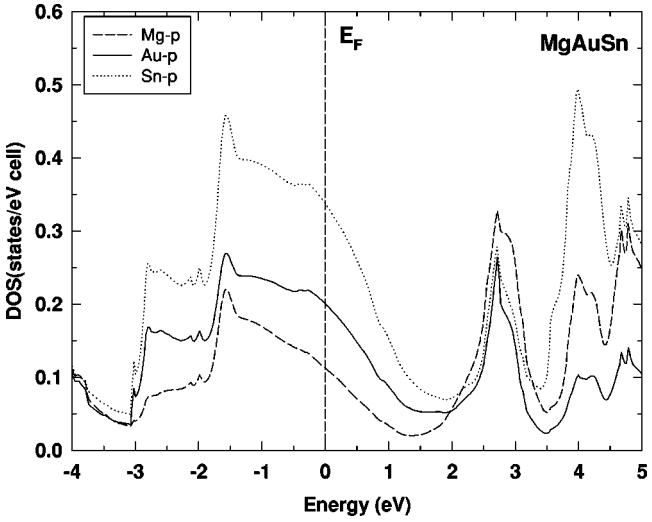

FIG. 6. Partial density of states for MgAuSn *p* states calculated from the TB-LMTO method.

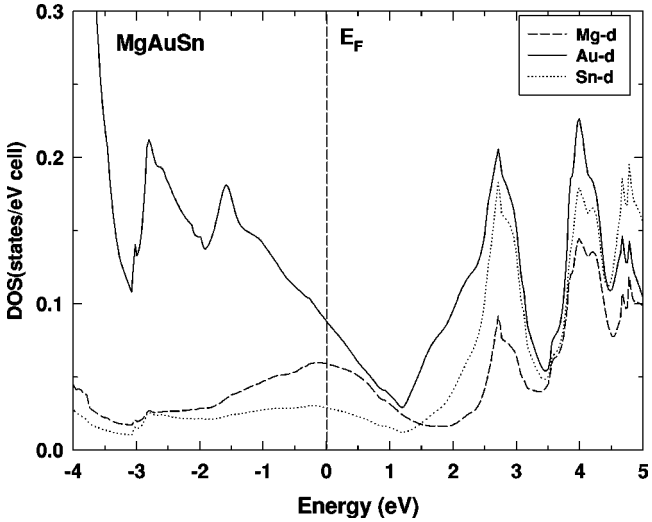

FIG. 7. Partial density of states for MgAuSn *d* states from the TB-LMTO method.

states. The partial densities of states for *p* and *d* states are plotted in Figs. 6 and 7. The Mg-*p*, Au-*p*, and Sn-*p* states show quite similar densities of states, except for different magnitudes. The magnitude of the Sn-*p* partial DOS is larger than those of Au-*p* and Mg-*p*. But for *d* states, the magnitude of the Au-*d* partial DOS is larger than those of Mg-*d* and Sn-*d* states, especially below the Fermi energy. The shape of the Au-*d* DOS below the Fermi energy is different from that of the other two *d*-states. Two peaks at -2.8 and -1.5 eV are observed for Au-*d* states while there are no noticeable peaks in Mg-*d* and Sn-*d* states below the Fermi energy. There are two large peaks in the density of states above the Fermi energy for both *p* and *d* states, the first at 2.7 eV and the second at 4.0 eV. Between these two peaks, there is a valley at 3.5 eV. Another valley exists between 1.5 and 2.0 eV as shown in Figs. 6 and 7. The Drude plasma energy can be obtained from the band structure.[21] The $N(E_F)$ and E_F from the TB-LMTO method were 0.95 states $\mathrm{eV}^{-1}\,\mathrm{cell}^{-1}$ and 10.13 eV, respectively. From these values, the obtained Drude plasma energy is 8.17 eV. This is fairly good agreement with the fitting value of 6.0 eV.

V. SUMMARY AND CONCLUSIONS

The optical conductivity spectrum of single-crystal of MgAuSn has been measured between 1.5 and 5.0 eV. It agrees well with the calculated values including both interband and intraband contributions. The interband contribution to the optical conductivity was obtained from the self-consistent TB-LMTO method based on the LDA formalism and the intraband contribution from the classical Drude model. The complex dielectric function was derived by including both contributions and compared with experimental data. The agreement of theory and experiment was good by including the intraband contribution due to the large negative free-electron gas contribution to ε_1 in the visible region. The electronic structure and the partial density of states of MgAuSn were calculated. From the *p* and *d* partial density of states of Sn, Au, and Mg, the peaks in the optical conductivity spectrum can be analyzed. The large peak at 2.9 eV is due to transitions from occupied *p* states to unoccupied *d* states 2.6 eV above the E_F. The small shoulder at 4.1 eV is due to occupied *p* states to unoccupied *d* states 4.0 eV above the E_F.

ACKNOWLEDGMENTS

Ames Laboratory is operated for the U.S. Department of Energy by Iowa State University under Contract No. W-7405-Eng-82. This work was supported by the Director for Energy Research, Office of Basic Energy Science.

[1] J. Drews, U. Eberz, and H.-U. Schuster, J. Less-Common Met. **116**, 271 (1986).
[2] P. C. Canfield and Z. Fisk, Philos. Mag. B **65**, 1117 (1992).
[3] GSAS Rietveld refinement program by A. C. Larson and R. B. Von Dreele, Los Alamos National Laboratory, Los Alamos, NM 87545.
[4] U. Eberz, W. Seelentag, and H. U. Schuster, J. Naturforsch, Teil B: Anorg. Chem. Org. Chem. **35**, 1341 (1980).
[5] R. M. A. Azzam and N. M. Bashara, *Ellipsometry and Polarized Light* (North-Holland, Amsterdam, 1977).
[6] D. E. Aspnes and A. A. Studna, Appl. Opt. **14**, 220 (1975).
[7] S. J. Lee, S. Y. Hong, I. Fisher, P. C. Canfield, B. N. Harmon, and D. W. Lynch, Phys. Rev. B **61**, 10 076 (2000).
[8] U. von Barth and L. Hedin, J. Phys. C **5**, 1629 (1972).
[9] R. Kubo, J. Phys. Soc. Jpn. **12**, 570 (1957).
[10] L. J. Sham and W. Kohn, Phys. Rev. **140**, A1133 (1965).

[11] J. E. Müller, O. Jepsen, and J. W. Wilkins, Solid State Commun. **42**, 365 (1982).
[12] F. Wooten, *Optical Properties of Solids* (Academic Press, New York, 1972).
[13] C. Kittel, *Introduction to Solid State Physics* (Wiley, New York, 1996), Chap. 10.
[14] H. Ehrenreich and H. R. Philipp, Phys. Rev. **128**, 1622 (1962).
[15] D. H. Seib and W. E. Spicer, Phys. Rev. Lett. **22**, 711 (1969).
[16] D. E. Weiss and L. Muldawer, Phys. Rev. B **10**, 2254 (1974).
[17] P. Winsemius, F. F. van Kampen, H. P. Lengkeek, and C. G. van Went, J. Phys. F: Met. Phys. **6**, 1583 (1976).
[18] L. Y. Chen and D. W. Lynch, Phys. Status Solidi B **148**, 387 (1988).
[19] A. Gupta and R. Gupta, Phys. Status Solidi B **168**, 456 (1991).
[20] I. I. Mazin, E. G. Maksimov, S. N. Rashkeev, and Yu. A. Upenskii, Zh. Eksp. Teor. Fiz. **90**, 1092 (1986) [Sov. Phys. JETP **63**, 637 (1986)].
[21] L. F. Mattheiss and J. C. Hensel, Phys. Rev. B **39**, 7754 (1989).